



Micropore structure and fractal characteristics of shale in Midwest China

Rui Shen¹ · Xiaoyi Zhang² · Hang Yang¹ · Huichen Ren¹ · Hekun Guo¹ · Hongtao Zhou¹

Received: 30 March 2023 / Accepted: 1 January 2024 / Published online: 7 February 2024
© The Author(s) 2024

Abstract

To further clarify the optimal target layer in the horizontal section of Wufeng–Longmaxi shale, we selected 126 shale samples from the Wufeng–Longmaxi Formations (Long₁¹ to Long₁⁴ and Long₂ submember) as the primary study objects from the perspective of the microscopic pore structure. We conducted this experimental study on the pore structure of shale samples according to various methods, including low-temperature nitrogen adsorption and carbon dioxide adsorption experiments, atomic force microscopy, and nano-computed tomography scanning. We calculated the fractal dimensions of samples at different horizons through the study of the characteristics of adsorption–desorption isotherms using the Frenkel–Halsey–Hill model. These results indicated that the shale samples had a complex pore structure (with a higher fractal dimension). The fractal dimensions were positively correlated with the specific surface area and total organic carbon content of the shale samples, weakly positively correlated with the micropore pore volume, and negatively correlated with the average pore radius. The samples from the Wufeng Formation and the Long₁¹ and Long₁² submembers had large fractal dimensions, whereas the samples from Long₂ had the smallest fractal dimension. The pores of the shale samples generally were type H2/3, which were characterized by wedge, tabular, and ink-bottle shapes. Only three H3-type pore samples corresponded to the three smallest fractal dimension values. The Wufeng Formation’s Long₁¹ and Long₁² layers should be the target layers for horizontal wells. In this study, we identified the optimal target layer of the horizontal shale profile of Wufeng–Longmaxi Formation, which holds great significance for shale oil and gas development in this formation.

Keywords Shale · N₂ adsorption · Pore structure · Fractal characteristics · Atomic force microscope

Abbreviations

AFM	Atomic force microscopy
BET	Brunauer–Emmett–Teller
CT	Computed tomography
FE-SEM	Field emission scanning electron microscopy
FHH	Frenkel–Halsey–Hill
FIB-SEM	Focused ion beam scanning electron microscope
IUPAC	International Union of Pure and Applied Chemistry
TEM	Transmission electron microscopy
TOC	Total organic carbon

List of symbols

C	Constant
D	Fractal dimension
F_s	Roughness and undulation of the plane
K	Slope of the logarithmic curve of $\ln(V)$
L	Length of scan range sample (μm)
p	Equilibrium pressure (MPa)
p_0	Saturation pressure (MPa)
R_n	Number of rows in the gray image matrix
V	Volume of N ₂ adsorption at each equilibrium pressure (cm^3)
W	Width of scan range sample (μm)
$x(i,j)$	Gray value of the pixel in the i row and the j column of image gray matrix

✉ Rui Shen
shenrui523@126.com

¹ Research Institute of Petroleum Exploration & Development, PetroChina Company Limited, Beijing, China

² North China Institute of Aerospace Engineering, Langfang, China

Introduction

Shale gas is formed by thermogenic and biogenic origins, and it is stored in a free gas form in pores and fractures (Liu et al. 2021). The adsorbed gas forms in organic matter or

clay minerals, and the dissolved gas forms in bitumen or kerogen (Hu et al. 2016). Because of the strong heterogeneity and anisotropy of shale and the diversity of gas occurrence, the flow mechanisms of shale gas are complex, including desorption, diffusion, and seepage (Chandra et al. 2022). Therefore, the porosity, specific surface area, and pore size distribution characteristics are important parameters used to characterize the pore structure of shale (Afagwu et al. 2023). Because of the high complexity of shale microscopic pore systems, Euclidean geometry cannot be used to describe and accurately characterize the shale microscopic pore systems (Afagwu et al. 2022). Therefore, it is necessary to integrate fractal geometry into the original system and to use the fractal method to study the pore characteristics of shale (Qiu et al. 2021; Seely et al. 2022; Zhu et al. 2021; Fan et al. 2022).

The common characterization methods for conventional porous solid pores include the fluid-intrusive method, image analysis method, and noninterference method (i.e., nonintrusive method) (Iqbal et al. 2021). The fluid-intrusive method is used to detect the connected pores in a sample by injecting fluid into the sample, including the low-temperature nitrogen (N_2) adsorption method, carbon dioxide (CO_2) adsorption method, and high-pressure mercury intrusion method (Fatah et al. 2022). The image analysis method has been used to establish an intuitive understanding of the reservoir structure through images with advanced imaging technology, including transmission electron microscopy (TEM), field emission scanning electron microscopy (FE-SEM), and atomic force microscopy (AFM). The nonintrusive method can be used to conduct nondestructive tests on samples, including nuclear magnetic resonance, small-angle scattering (SAS), and computed tomography (CT). Because the pore size distribution in shale is heterogeneous, and the span of pore size distribution is large (Chandra et al. 2023), these methods all have some limitations (Mudoi et al. 2022). The high-resolution backscatter image method is limited by its magnification. Although the pore shape of the image can be observed, it is difficult to accurately characterize the complex pore characteristics of shale (Pang et al. 2021). The electron microscopy method is relatively high in resolution, at the nanometer level, but it cannot realize a full-scale quantitative description. The gas adsorption method is limited in its test range (Wang et al. 2021). For example, the pore diameter range of the low-temperature N_2 adsorption test is 1.2–200 nm, and that of the CO_2 adsorption test is ≤ 2 nm. During high-pressure mercury intrusion testing, because of the complex pore structure, diverse pore shapes, and micropore development in shale, the saturation of mercury is frequently low, and most pores cannot be analyzed using this method (Chandra et al. 2022). Scholars have noted that high pressure may cause the deformation and damage of pore structures (Medina et al. 2023). Therefore, it is difficult to effectively

characterize the multiscale pore structure and pore size distribution of shale using a single method (Pitcher et al. 2021).

Using the AFM method, the surface structure and properties of substances can be studied by detecting the extremely weak interatomic interaction between the surface of the sample to be tested and a miniature force-sensitive element. While scanning the sample, the sensor can detect these changes, and the force distribution information can be obtained. Therefore, the surface topography structure and surface roughness information can be obtained at the nanometer resolution. AFM has been widely used in nanotechnology studies in the fields of materials science, biology, physics, data storage, semiconductors, polymers, chemistry, and biological materials, but it is rarely used in the study of shale pore structure (Liu et al. 2021; Shen et al. 2021a, b; Zhang et al. 2020).

Among the fluid-intrusive methods, the low-temperature N_2 adsorption method currently is the most widely used method for the quantitative characterization of the micropore structure of tight reservoirs, and it can be used to effectively characterize pores between 1.2 nm and 200 nm. Scholars have carried out a large number of studies using low-temperature N_2 adsorption experiments (Xu et al. 2019). Han et al. compared the influence of sample particle size and water content on N_2 adsorption (Han et al. 2016). Zapata and Yang obtained information about the influence of the properties of sorbents and adsorbates on nitrogen adsorption by studying N_2 adsorption isotherms (Yang et al. 2023; Zapata and Sakhaee-Pour 2016). Many scholars also have analyzed the N_2 adsorption capacity and described the correlations among sample surface area, pore volume, pore type, and other factors (Chao et al. 2016b, a; Chen et al. 2018). In the study of Longmaxi Formation shale, scholars generally believe that the fractal dimension is positively correlated with total organic carbon (TOC), micropore development degree, vitrinite reflectance (R_o), clay mineral content, and Brunauer–Emmett–Teller (BET) specific surface area (Yang et al. 2023). The fractal dimension is negatively correlated, however, with feldspar content, average pore size of the sample, and pore volume (Saeed et al. 2022; Fu et al. 2021; Chen et al. 2021; Blach et al. 2021). The high-pressure mercury intrusion capillary pressure method is another common fluid intrusion method (Shen et al. 2021a, b; Liu et al. 2021; Li et al. 2018a, b; Han et al. 2020; Zhang et al. 2020; Cai et al. 2018).

To date, most studies on pore structure and fractal dimension do not specify the subsection and small-layer position of the core or whether the core samples are taken from the primary production layers. In addition, the number of samples has been small, and the samples have demonstrated weak representativeness, resulting in significant differences in the study of shale in the same area. For example, scholars still dispute the correlation between the fractal dimensions

and pore volume of Longmaxi Formation shale (Xiong et al. 2022).

Pore fractal dimension is important for understanding the complex geological structure, stratigraphic characteristics and reservoir modeling. Firstly, pore fractal dimension can describe the complexity and irregularity of pore structure. Pore structure is the main carrier of fluid storage and flow in the formation. The complexity and irregularity of pore structure can be analyzed by fractal dimension, which is helpful to understand the reservoir characteristics and fluid flow characteristics of strata. Secondly, pore fractal dimension has an important application in reservoir modeling. By incorporating pore fractal dimension into the modeling process, the flow of oil and gas in the formation can be simulated more accurately, the development effect can be predicted, and more effective development technology strategies can be formulated.

In this study, we summarized a large amount of data and studied the fractal characteristics of the four sublayers of the Long₁ submember of the Longmaxi Formation, the Long₂ submember, and the Wufeng Formation shale using N₂ adsorption experiments. We used AFM and nano-CT to study the pore distribution characteristics and the connectivity of shale samples. AFM and nano-CT have been used to study the pores, throat distribution, and connectivity of pores < 800 nm and ≥ 800 nm as well as to comprehensively study correlations among the pore-throat configuration and three-dimensional (3D) spatial fluctuation degree and fractal dimension to provide the necessary experimental basis for the sweet-spot selection, resources evaluation, and development of shale gas reservoirs. In this study, we combined the cryogenic N₂ adsorption experiment and AFM to provide evidence for the determination results of hysteresis loops through the high-resolution display of AFM. We also proposed a more accurate hybrid hysteresis loop type, which made the description of pore morphology more accurate. This work filled the technical gap in the low-temperature N₂ adsorption method, which can be used to determine pore morphology only qualitatively and lacks supporting evidence.

Materials and methodology

Experimental samples

Marine shale in Sichuan Basin is the most realistic field of shale gas exploration and development in China. Shale gas development has basically formed targeted shale gas well production, production and gathering, and transportation technology. The well station gathering and transportation process can meet the needs of shale gas development. The Changning–Weiyuan Shale Gas Demonstration Zone is

located in the southern part of Sichuan Province, which is the location of the main commercially developed shale gas fields. The gas fields are characterized by overpressure with a pressure coefficient of 1.2–2.0. The area of the demonstration region is 6534 km² with proven shale gas reserves of more than 300 billion m³.

The Wufeng Formation and Long₁ Formation are high-quality reservoir sections and the main gas-producing layers of shale gas in Sichuan Basin. The small layers of Long₁¹ to Long₁⁴ in the Long₁ submember of the Long₁ Formation are the main target layers for horizontal well development. A total of 126 core samples have been recovered from the Wufeng–Longmaxi Formations (Long₁¹ to Long₁⁴ and Long₂ submembers) in Changning, Weiyuan, Dazu, and other established production areas (Fig. 1). Basic parameters, such as porosity and permeability of core samples, are shown in Fig. 2. The porosity and permeability of the samples in the same small layer are approximately positively correlated with the depth.

Experimental method

The low-temperature nitrogen adsorption experiment can calculate the pore volume distribution of shale by measuring the adsorption amount of nitrogen under different pressures and characterize the size range and number of pores. In addition, the specific surface area can be calculated and the pore morphology can be judged by the adsorption–desorption curve. Atomic force microscopy can observe and measure the morphology of shale pores at the nanometer scale, and the distribution of pore scale can be obtained by statistical analysis of a large number of scanned image data. It is very important to evaluate the permeability and fluid transport capacity of shale by scanning the motion path of the probe and observing the connection between pores to help understand the connectivity of the pore network. The atomic force microscope can also understand the physical and chemical properties of the pore surface by measuring the interaction force between the probe and the pore wall. For example, parameters such as surface roughness, hardness, and adhesion can be measured to reveal the morphology and surface characteristics of the pore wall. The comprehensive utilization of low-temperature nitrogen adsorption and atomic force microscopy is of great significance for understanding the reservoir characteristics, permeability and fluid transport capacity of shale.

Low-temperature N₂ adsorption and desorption experiment

We used the Autosorb-6B adsorption instrument made by Quantachrome Corporation USA in the experiment. With a voltage of 100–240 V, 50/60 Hz, six samples could be

information as well as other physical quantity information. During the experiment, we first used an optical microscope to determine the area polished by argon ion. Then, we used the AFM for detection. Finally, we scanned multiple areas to obtain more comprehensive data. The sample dimensions were $10 \times 6.5 \times 2$ mm. We used a grinding and polishing machine to process the to-be-scanned surface and the reverse surface of each sample and then used 3000-grit sandpaper to further polish the surface to be scanned. Finally, we used argon ion milling to smooth the surface so that it met the requirements for roughness measurement using AFM.

CT and 3D reconstruction

CT uses cone-beam X-rays to penetrate the object and to reconstruct a 3D model with a large number of X-ray attenuation images obtained by rotating the core 360 degrees. In this study, we used the Phoenix Nanotom Nano-CT instrument by General Electric, with a resolution of 300 nm. The advantages of nano-CT core analysis are that it can fully display the small features of the surfaces using a large amount of image data without destroying the sample and the CT image can reflect the information of the energy attenuation of the X-ray during the process of penetrating the object. The pore structure and relative density inside the core are positively correlated with the gray level of the 3D CT image. During the experiment, the sample taken by a 1-mm-diameter drill was placed on the stage of the CT instrument for CT scanning after adjusting the scanning parameters. After scanning, the digital 3D model could be reconstructed by reducing the effects of artifacts and beam hardening. Finally, using professional data processing software (e.g., VGSTUDIO MAX and FEI Avizo), we processed and analyzed the reconstructed 3D model, including pore and fracture extraction analysis of cores, pore-throat connectivity analysis of cores, internal display of the 3D view (e.g., distribution of internal pores, fractures, and organic matter), histogram of pore size distribution, and 3D animation of core fault slices.

Results

The heterogeneity of pores indicates the complexity of the size, number, distribution, and type of pores in shale, which determines the storage capacity of shale reservoirs. The fractal dimension D is a quantitative index that can characterize the roughness or complexity of a solid surface, with values ranging from 2 to 3. The closer the value is to 3, the rougher or more complex the shale. A larger fractal dimension is more favorable for gas adsorption and less favorable for gas seepage. Therefore, the fractal dimension can be used to not only describe the geometric shape and structural

properties of shale but also evaluate the heterogeneity of shale reservoirs.

Fractal dimension calculation method

According to the experimental data of low-temperature N_2 adsorption, we determined the fractal dimension using the Frenkel–Halsey–Hill (FHH) model. The calculation formula is as follows (Medek and Weishauptová 2000):

$$\ln(V) = K \cdot \ln[\ln(p_0/p)] + C, \quad (1)$$

where p is the equilibrium pressure, MPa; p_0 is the saturation pressure, MPa; V is the volume of N_2 adsorption at each equilibrium pressure p , cm^3/g ; C is a constant; p_0/p is the reciprocal of the relative pressure; K is the slope of the logarithmic curve of $\ln(V)$; and $\ln[\ln(p_0/p)]$.

On the basis of previous conclusions, when monolayer or multilayer molecular adsorption occurs on the sample surface, the primary force is van der Waals force, which corresponds to $0 < p/p_0 < 0.45$ in the sample adsorption isotherm curve. At this time, the correlation between K and fractal dimension D is as follows:

$$D = 3K + 3. \quad (2)$$

When capillary condensation occurs on the surface of the sample, the primary force is surface tension, which corresponds to $0.45 < p/p_0 < 0.9$ in the adsorption isotherm curve of the sample. At this time, the correlation between K and fractal dimension D is as follows (Avnir and Jaroniec 1989):

$$D = K + 3. \quad (3)$$

The sample had a hysteresis loop when the relative pressure was about 0.45, and capillary condensation would occur within the pores. Therefore, we selected the adsorption data after the separation of the adsorption curve and desorption curve. At the same time, when the relative pressure was close to 1, the adsorption data were inaccurate because of the influence of the accuracy of the instrument. Therefore, we removed this part of data when calculating the fractal dimension. After removal, the graph correlation coefficient R^2 significantly improved, and the average of each sample was 0.9812. Finally, by combining with formula (3), the calculation formula of fractal dimension can be obtained, as follows:

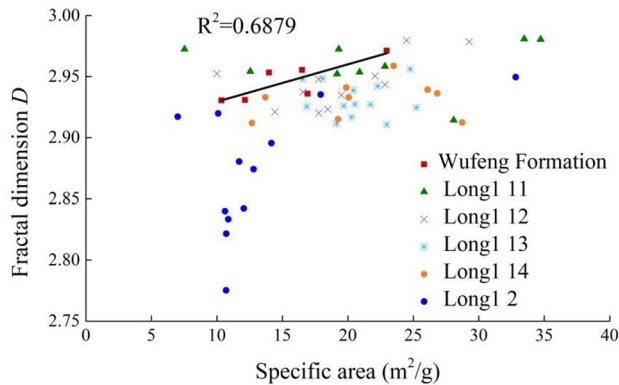
$$\ln(V) = (D - 3) \cdot \ln[\ln(p_0/p)] + C. \quad (4)$$

Characteristics of fractal dimension

We selected 67 shale samples from different wells and different horizons, which were then classified according to the

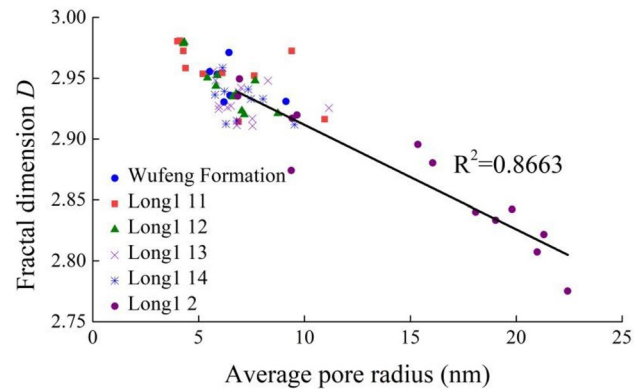
Table 1 Fractal dimension of shale samples in different horizons

Sample type	Fractal dimension	Wufeng	Long1 ₁ ¹	Long1 ₁ ²	Long1 ₁ ³	Long1 ₁ ⁴	Long1 ₂
I	≥ 2.95	42.86%	69.23%	33.33%	7.69%	11.11%	0
II	2.90~2.95	57.14%	30.77%	66.67%	92.31%	88.89%	69.23%
III	≤ 2.9	0	0	0	0	0	30.77%
Sample number	6	0	11	13	9	12	Sample Number
Mean	2.9462	2.9525	2.9444	2.9309	2.9311	2.8737	Mean

**Fig. 3** Correlation between specific surface area and fractal dimension of the shale samples

horizons. We measured the specific surface area and average pore radius of the sample. According to the fractal dimension $D \geq 2.95$, $D = (2.90 \sim 2.95)$, $D \leq 2.90$, we categorized the samples as Type I, Type II, and Type III. We obtained the proportion of each type of sample in each layer and calculated the average fractal dimension of the sample (Table 1). These results indicated that the specific surface of the sample increased with the increase in pores and the decrease in average pore radius. Thus, with an increase in micropores in the shale samples, the pore structure became more complicated. The larger the fractal dimension of shale, the more favorable the gas adsorption in the sample. Among the samples, the Wufeng Formation, Long1₁¹, and Long1₁² samples had larger fractal dimension values, with good gas storage capacity. Only the Long1₂ contained Type III samples, which had the worst gas storage capacity.

Although most scholars believe that the fractal dimension of shale samples is positively correlated with specific surface area, in our research, we found that the correlation between specific surface area and fractal dimension was not obvious. Among the samples, only the Wufeng Formation had a relatively strong positive correlation, with the correlation coefficient $R^2 = 0.6879$ (Fig. 3). For comparison, the correlation coefficient R^2 of Long1₁¹ to Long1₁⁴ and Long1₂ was as follows: 0.1490, 0.3617, 0.0008, 0.0511, and 0.2656. Therefore, based on our existing data, the fractal dimension of the shale samples did not have an obvious correlation or a weak positive correlation with specific surface area.

**Fig. 4** Correlation between average pore radius and fractal dimension of the shale samples

Note, however, that only the values of the pore volume in the Wufeng Formation were similar. It is natural to doubt whether the positive correlation would become clear if the pore volume was similar. Furthermore, we reviewed the data for similar pore volume and found that the positive correlation increased visibly except for the Long1₁¹ Formation. It was interesting that the Long1₁¹ Formation showed a negative correlation between specific surface area and fractal dimension. More research is needed to explain whether this was caused by accidental sampling or whether this layer truly had different properties. Based on most of the data, it was very possible that a weak positive correlation existed between specific surface area and fractal dimension, and the positive correlation became stronger when the pore volume of the samples became closer. The average pore radius of the sample and fractal dimension was negatively correlated with fractal dimension as a whole. Among the samples, the average pore radius of the samples from the Long1₂ was most negatively correlated with fractal dimension, with a correlation coefficient $R^2 = 0.8663$ (Fig. 4).

By taking 16 shale samples from different wells and different horizons from the samples, we measured the TOC content of the samples to analyze the correlation of TOC with the fractal dimension. The results indicated that the TOC was positively correlated with fractal dimension, with a correlation coefficient $R^2 = 0.6497$ (Fig. 5). The samples from the Wufeng Formation, Long1₁¹, Long1₁², and Long1₁³ had a higher organic matter content and a

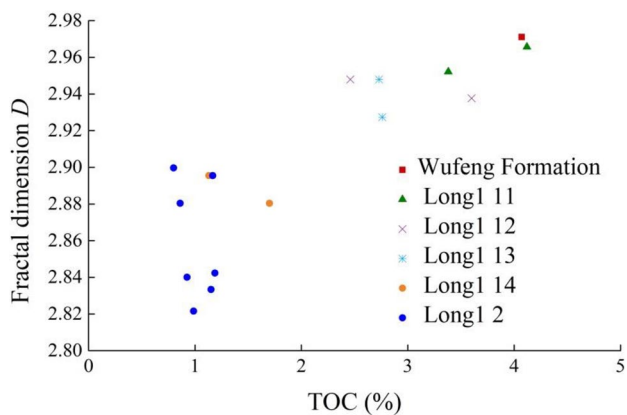
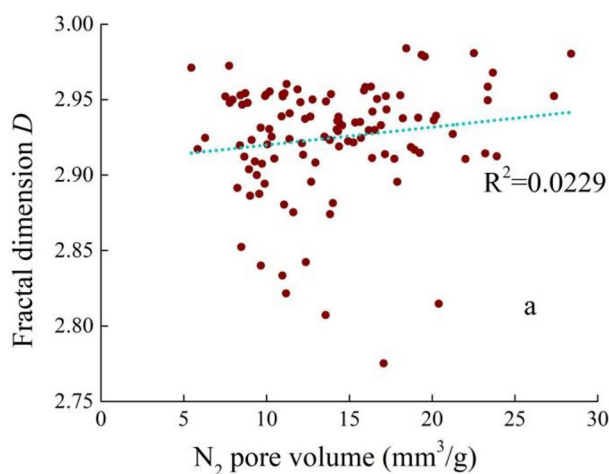


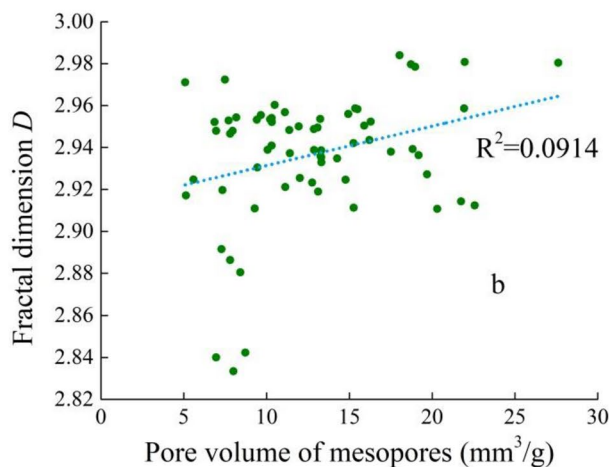
Fig. 5 Correlation between TOC and fractal dimension of the shale samples

larger fractal dimension. These results indicated that the higher the organic content, the more evident the increase in mesopores, the more complex the pore structure, and the larger the fractal dimension.

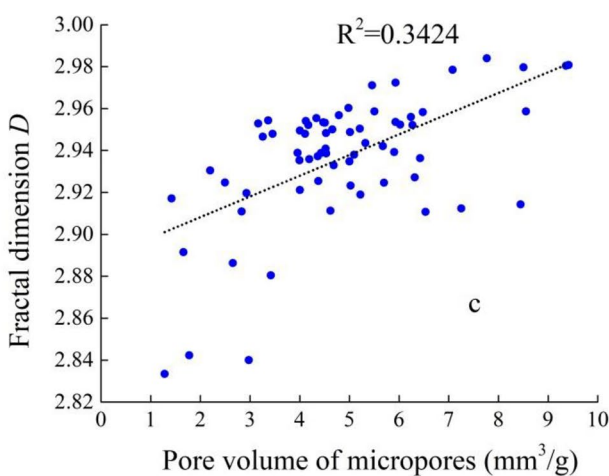
In previous studies, the correlation between fractal dimension and pore volume has been controversial. In this study, we conducted an N_2 adsorption experiment to measure the total pore volume of all 126 shale samples with a pore diameter of 1.2–100 nm, and then, we selected 66 shale samples from different wells and different layers and conducted the N_2 adsorption experiment and the CO_2 adsorption. In these experiments, we simultaneously measured the pore volume of mesopore (2–50 nm) and micropore (< 2 nm). Figure 6a–c, respectively, shows the relationship between fractal dimension D and N_2 pore volume, pore volume of mesopores and pore volume of micropores. N_2 point volume is the pore volume measured in the low-temperature nitrogen adsorption experiment, that is, the pore volume corresponding to the pore diameter of 2–200 nm, the pore volume of mesopores is the pore volume corresponding to the pore diameter of 2–50 nm, and the pore volume of micropores is the pore volume corresponding to the pore diameter of ≤ 2 nm. We found that the N_2 pore volume and mesopore volume evidently were not correlated with fractal dimension, with correlation coefficients R^2 of 0.0229 and 0.0914 (Fig. 6a, b), respectively. In comparison, we found only a weak positive correlation with micropore volume with a correlation coefficient R^2 of 0.3424 (Fig. 6c). This result indicated that the pore complexity of the Longmaxi Formation shale was mainly due to the contribution of micropores. Although this relationship has been controversial in previous studies, based on our data, we concluded that a correlation did not exist between fractal dimension and pore volume and that only a weak positive correlation existed with micropore volume.



(a)



(b)



(c)

Fig. 6 Correlation between pore volume and fractal dimension of the shale samples

Comparison of fractal dimension between shale and other lithologies

We selected five shale samples from Well Wuxi 2 and compared these samples with the six mudstone samples from Daqing reservoir and six sandstone samples from Mahu reservoir in Xinjiang, China. The parameters of the samples, including specific surface area and pore volume, are given in Table 2. We found that the fractal dimension of shale was higher than that of mudstone and sandstone. These results indicated that the pore structure of shale was the most complex. The specific surface of shale and mudstone was positively correlated with the fractal dimension, and the average pore radius was negatively correlated with the fractal dimension (Fig. 7). The fractal dimension of sandstone was not correlated with the specific surface and average pore radius.

Low-temperature N₂ adsorption/desorption hysteresis loop type

The adsorption isotherm curve can be divided into three sections according to the adsorption process, namely the low-pressure section ($0 < p/p_0 < 0.45$), the middle-pressure section ($0.45 < p/p_0 < 0.8$), and the high-pressure section ($0.8 < p/p_0 < 1$). At the low-pressure section, the curve rose slowly, with a strong force between the sample and nitrogen, which was mainly monolayer adsorption, and the adsorption–desorption isothermal curve was relatively approached. At the middle-pressure section, according to the BET equation, the curve rose slowly, reflecting the gradual filling of

the micropores, which was mainly multimolecular layer adsorption. When the adsorption layer was thick enough, capillary condensation occurred. At the high-pressure section, the curve rose sharply, reflecting that the sample had macropores and mesopores, which corresponded to the capillary condensation stage (Pfeifer et al. 1989). By studying adsorption isotherms, it is possible to obtain information on the properties of adsorbents and adsorbates (Zapata and Sakhaee-Pour 2016; Hu et al. 2016; Chao et al. 2016b, a). The desorption process, however, was caused only by capillary condensation. When desorption was at the same relative pressure as adsorption, only vapor on the capillary liquid surface could be desorbed. A smaller relative pressure was required to desorb the adsorbed molecules. Therefore, the hysteresis of desorption appeared, which resulted in the formation of a hysteresis loop.

Because the hysteresis loop is related to the capillary condensation in the pores, each type of hysteresis loop can correspond to certain pore structure characteristics. The International Union of Pure and Applied Chemistry (IUPAC) has classified four types of adsorption isotherms, which are designated H1 to H4 (Fig. 8), corresponding to cylindrical pores, bottleneck pores, wedge-shaped pores, and fracture-shaped pores (Sing 2013). The H1 hysteresis loop was narrow, and the adsorption and desorption branches were perpendicular to the pressure axis and parallel to each other, which corresponded to the narrow cylindrical pores open on both ends. The H2 hysteresis loop was relatively wide, and the desorption branch was extremely gentle at the beginning. At the middle pressure, it became steep, corresponding to

Table 2 Fractal dimension of shale samples in different horizons

Number	Lithology	Place of origin	Specific surface area (m ² /g)	Pore volume (mm ³ /g)	Average pore radius (nm)	Fractal dimension D
28–4	Shale	Wuxi 2	15.456	8.470	7.574	2.8523
29–4			20.364	11.610	5.519	2.8753
30–4			22.505	9.718	4.859	2.9075
31–4			22.456	9.302	5.025	2.909
32–4			20.849	9.888	4.560	2.8943
1	Mudstone	Daqing	35.374	35.795	11.368	2.852
8			9.061	16.136	14.651	2.7774
9			9.493	20.193	15.074	2.7525
20			36.073	37.239	10.317	2.862
24			56.772	56.545	8.249	2.8729
29	16.951	21.814	13.277	2.7914		
M604-1	Sandstone	Mahu	3.034	7.276	14.910	2.7748
M604-2			3.094	7.274	15.867	2.774
M604-3			4.640	12.193	14.056	2.7796
M604-4			3.565	9.353	16.145	2.7901
M604-5			3.568	10.170	14.405	2.7611
M604-6			2.815	6.524	14.032	2.8101

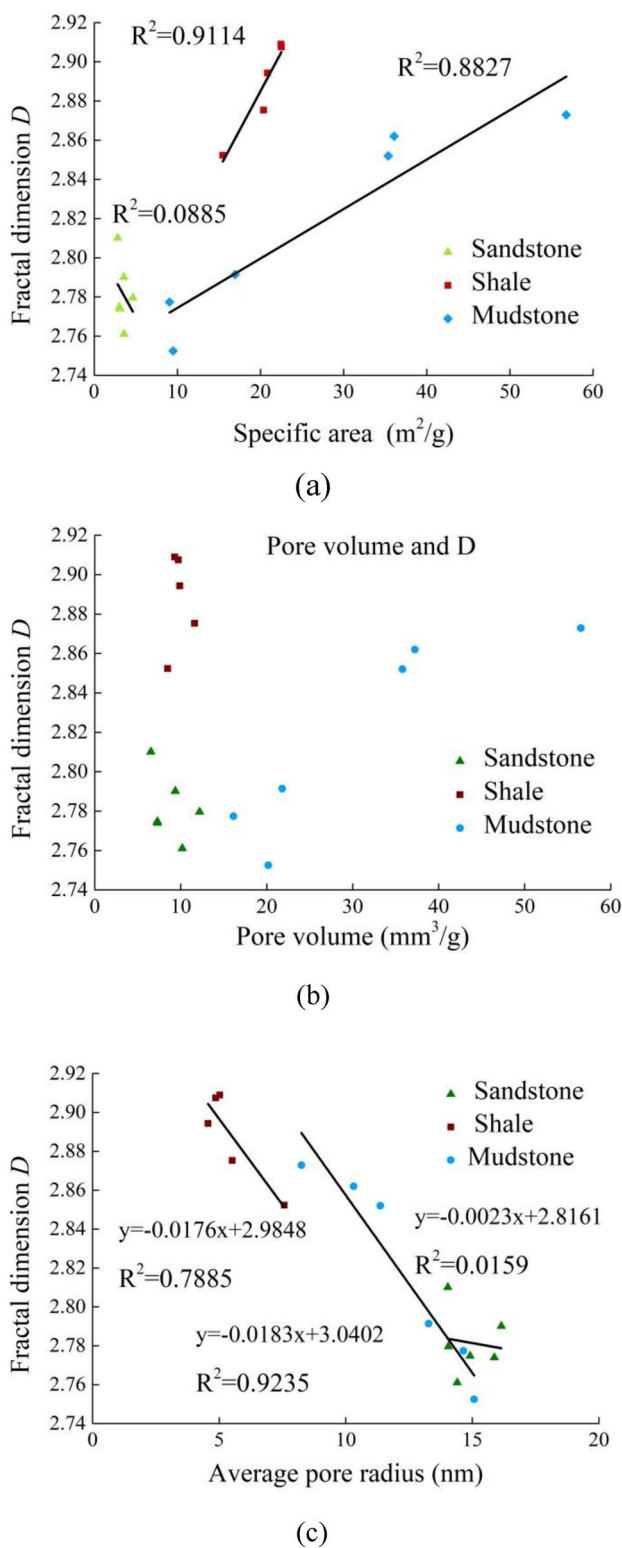


Fig. 7 Correlations among fractal dimension, specific surface area, and average pore radius of different lithology samples

ink-bottle-shaped pores. The adsorption branch of the H3 hysteresis loop rose slowly in the middle–low-pressure section and became steeper when the relative pressure increased, which corresponded to wedge-shaped and tabular pores. The adsorption and desorption branches of the H4 hysteresis loop remained parallel to the pressure axis and were parallel to each other under most relative pressures, which corresponded to slit pores.

Hysteresis loop and AFM

The hysteresis loop of shale samples was not a single type, but it was mostly a combination of two types. Of the three main types of samples, the primary type was H2/3, and the minority type was H3 and H2/4 (Fig. 9). Type H2/3 had pore characteristics of both types H2 and H3, which indicated that the pores in the sample were wedge-shaped and tabular pores. Type H2/3 had the characteristics of a narrow-necked ink-bottle shape, which is favorable for gas storage and absorption, but it is not favorable for gas seepage and desorption. These pore types were extremely complicated. Type H3 corresponded to single wedge-shaped and tabular pores, with good connectivity. Type H2/4 had the characteristics of types H2 and H4, which indicated that the pores in the sample were mainly slit pores, coupled with the characteristics of a narrow-necked ink-bottle shape.

These three pore types also were shown in the AFM results (Fig. 10). Figure 9 shows that the curves of a, b, and c corresponded to the type H2/3, H3, and H2/4 pores, respectively, obtained from the N₂ adsorption experiment. Thus, we found that the H2/4 hysteresis loop appeared in the samples of the Wufeng Formation and Long₁¹, which corresponded to a larger fractal dimension. The H3 hysteresis loop appeared in only three samples of the Long₁² submember, which corresponded to the smallest three fractal dimension values, namely 2.7752, 2.8073, and 2.8216. This result indicated that the samples with tabular and wedge-shaped pores were relatively simple in pore structures, with small fractal dimension and strong seepage capacity, but they were relatively poor in gas storage capacity.

We investigated the pore and throat distribution of five core samples taken from the four sublayers of Long₁⁴, Long₁³, Long₁², Long₁¹, and Wufeng Formation by CT scans and 3D reconstructions (Figs. 11 and 12). The pores of Long₁³, Long₁¹, and Wufeng Formation were relatively well developed, providing a broad space for gas occurrence (Fig. 13). The throats of the Long₁¹ layer and Wufeng Formation were relatively developed, and there were large slit-shaped pores, which provided channels for gas diffusion and seepage (Fig. 14). The storage and seepage spaces were best developed in the Long₁¹ layer and Wufeng Formation. They are the target layers for the development of staged fractured horizontal wells in this area. The Long₁³ layer could be

Fig. 8 Types of hysteresis loops

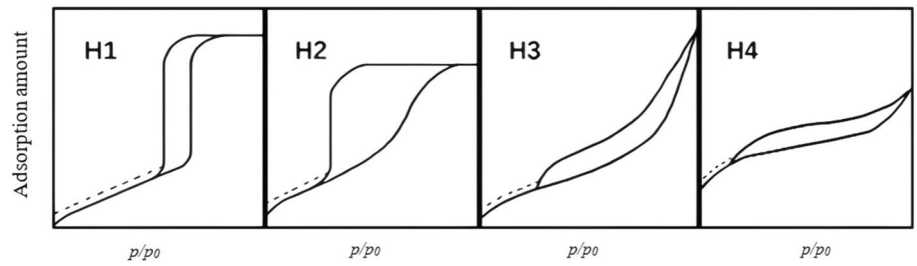


Fig. 9 Types of hysteresis loops of the shale samples

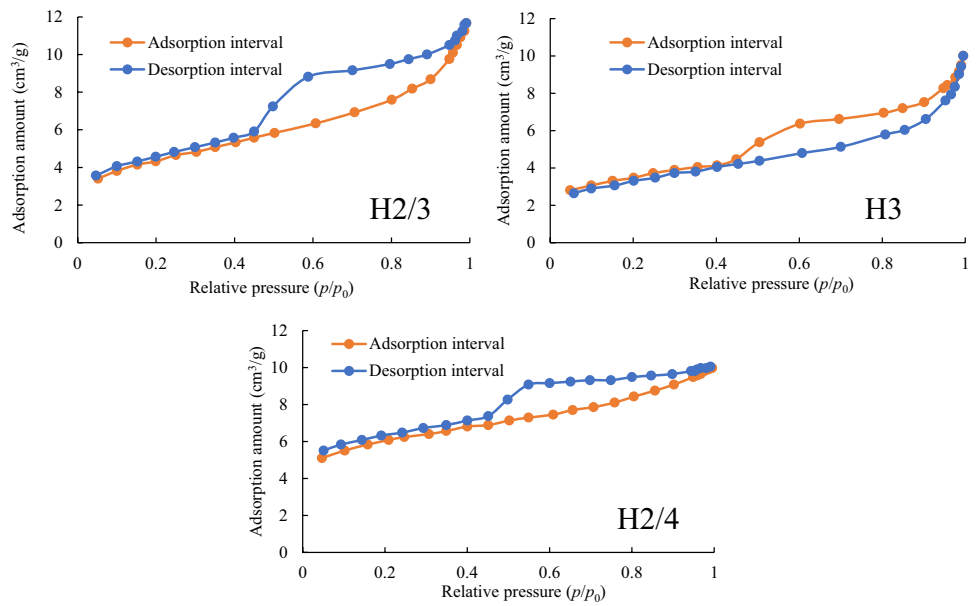


Fig. 10 Pore types shown under AFM

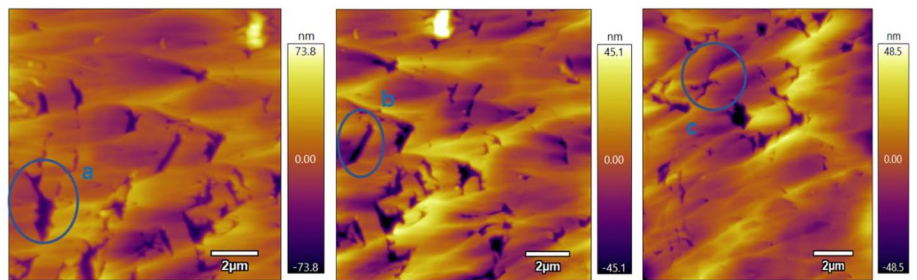


Fig. 11 Pore distribution by nano-CT

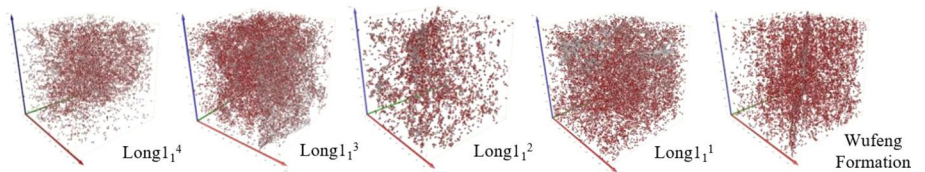


Fig. 12 Throat distribution by nano-CT

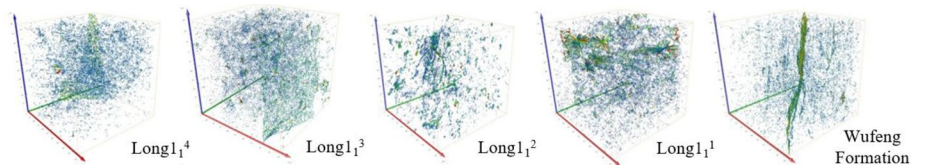
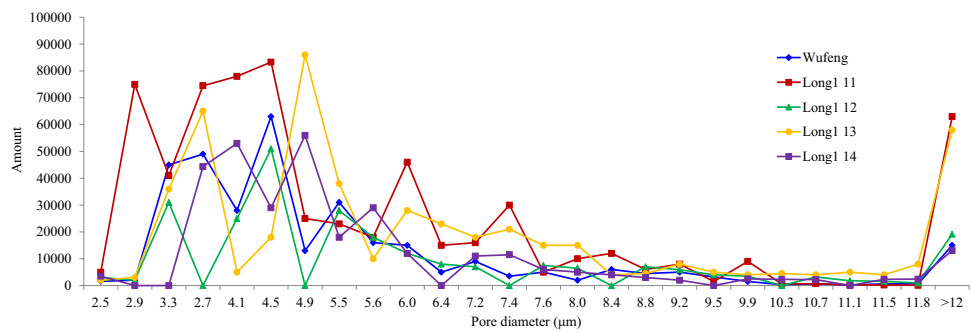
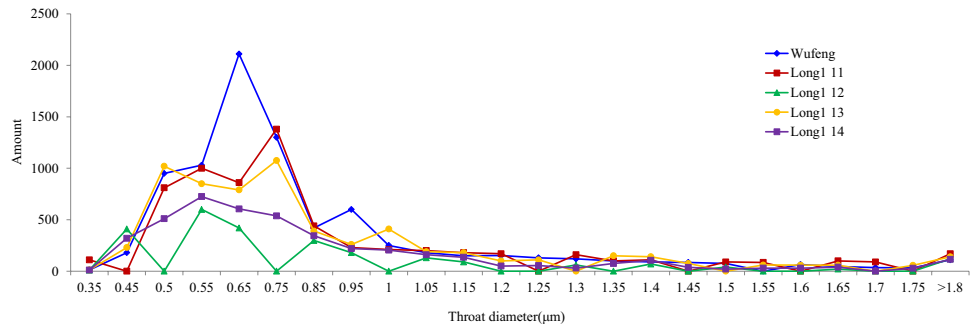


Fig. 13 Pore size distribution curves**Fig. 14** Throat size distribution curves

used as the target layer for productivity replacement or 3D development.

AFM and focused ion beam SEM

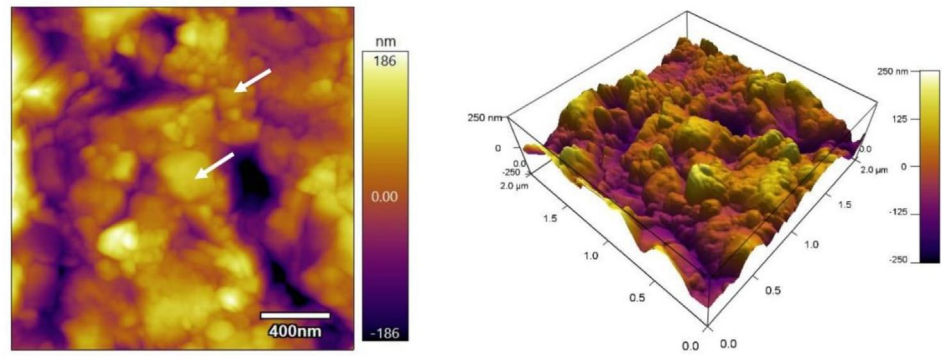
By observing the 3D morphology of shale samples obtained by JupiterXR AFM (Fig. 15a), we found that the shale samples had abundant storage space, with a large number of micro- and nanoscale pores, dense particle distribution, and deep space, which provided a wide range of space for gas occurrence. The large-scale enrichment of micro- and nanoscale pores was favorable for the storage of free gas. By contrast, because of the complexity of the surface of the shale sample, the specific surface of the sample was huge, which also provided substantial space for gas adsorption. JupiterXR AFM has high resolution, and both macropores and micropores can be clearly observed. The shale samples had abundant nanoscale pores and several microscale pores. The micron-scale pores and nanoscale pores connected to form a pore network through relatively small throats, which revealed the good connectivity of the micro- and nanoscale pores in shale reservoirs, providing channels for gas seepage into macropores and fractures. The focused ion beam (FIB) FE-SEM requires pretreatment processes, such as argon ion polishing and gold coating on the surface of the sample. The nanoscale throat could not be observed in the FE-SEM image (Fig. 15b). Therefore, AFM was more suitable for the observation of the pore structure of the shale samples.

Furthermore, it was difficult to observe the throat and study the coordination of pores and throats using FIB-SEM. With AFM, we observed the pore-throat network composed of pores and throat coordination and described the characteristics of pore-throat coordination. The pore-throat coordination number was the number of throats connected by a central pore and was the parameter used to describe the degree of connectivity between pores. The larger the pore-throat coordination number, the better the reservoir properties. The pore-throat coordination number could be calculated through image processing of the AFM. The pore-throat coordination numbers of the shale samples were 3, 4, and 5, which accounted for 23.4%, 29.9%, and 22.1%, respectively (Fig. 16), and the connectivity of the pore-throat network was good.

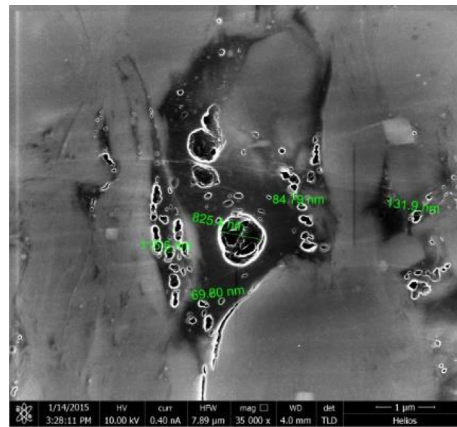
Roughness fluctuation and fractal dimension

First, we converted the AFM image of the rock sample into a gray image, and then, we read the image data information by MATLAB software. We calculated the trajectory curve of the AFM probe sweeping any line of the sample according to the depth data corresponding to the pixel. The fluctuation degree of the sample surface F_s and the spatial fluctuation degree F_i can be expressed as follows:

Fig. 15 Images of AFM and FIB-SEM



(a) AFM image of shale



(b) FIB-SEM image of shale

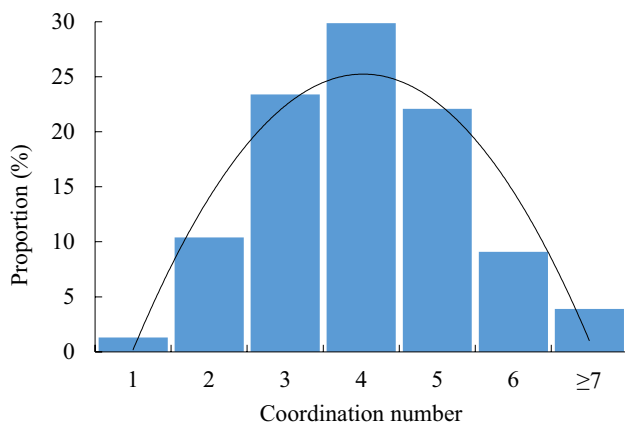


Fig. 16 Distribution histogram of pore-throat coordination number

$$F_s = \frac{\sum_{i=1}^{R_n} \sum_{j=1}^{R_n-1} \sqrt{\left(\frac{L}{R_n-1}\right)^2 + \left\{\frac{H}{255} [x(i, j+1) - x(i, j)]\right\}^2}}{LR_n}, \quad (5)$$

where F_s is the roughness and undulation of the plane, that is, the surface area scanned by the probe per unit plane area;

$x(i, j)$ is the gray value of the pixel in the i row and the j column of the image gray matrix; R_n is the number of rows in the gray image matrix; and L and W are the length and width, respectively, of the scan range sample, μm .

Roughness fluctuation degree is a measure of the degree of roughness and fluctuation of the inner surface of a pore relative to the average surface. Fractal theory has been widely used to describe and quantitatively characterize the shape and distribution characteristics of complex objects. It is also increasingly used to characterize rock pore size distribution and morphologies of pore and particle. Fractal dimension is the primary indicator used to measure the complexity and irregularity of objects. The models commonly used to calculate the fractal dimension include the FHH model, Menger sponge model, BET model, and thermodynamic method (Liu and Ostadhassan 2017; Li et al. 2018a, b; Cao et al. 2016; Sakhaee-Pour and Li 2016). The obtained fractal dimensions calculated from different models were not directly comparable, but the fractal dimensions calculated using the same model for different shales reflected the differences in the pore structure of shale. These results are convenient for the direct comparison of pore complexity of the shale reservoir and for the study of pores with different origins.

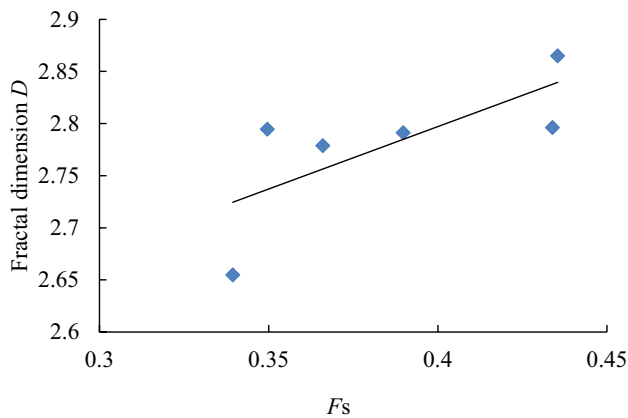


Fig. 17 Fractal dimension and spatial fluctuation roughness

In this study, we used the FHH model based on the experimental data of low-temperature N_2 adsorption to calculate the fractal dimension of Yuxi shale samples. We found that the fractal dimension was positively correlated with the spatial fluctuation roughness (Fig. 17). The results showed that the spatial roughness, volume complexity, and fractal dimension of the pore surface in the rock increased because of surface distortion and folding.

Discussion

Previously, the pore morphology of samples was qualitatively judged mainly by the type of hysteresis loop of low-temperature N_2 adsorption and visual evidence was lacking. In this study, we combined the low-temperature N_2 adsorption experiment and AFM and used the high-resolution display of AFM to provide evidence for the determination results of hysteresis loops. We also proposed a more accurate type of mixed hysteresis loop, ensuring that the description of pore morphology was more accurate.

The temperature of the low-temperature N_2 adsorption experiment was $-195\text{ }^\circ\text{C}$. Currently, relevant research is lacking on whether the low temperature has an impact on pore structure, which is also an important factor that may cause experimental bias. In addition, the low-temperature N_2 adsorption experiment used rock powder samples, which usually were 20–60 mesh in size. The different mesh numbers of the samples also can have an impact on the pore size distribution data. The resolution of AFM can reach 0.1 nm, which is very high and thus is suitable for studying the surface morphology, surface roughness, and Young's modulus of shale samples. Currently, however, the AFM experimental results lack fractal analysis methods, and relevant analysis methods are urgently needed.

Conclusions

In this study, based on AFM and a low-temperature N_2 adsorption experiment, we revealed the pore morphology of shale. Taking 126 shale samples from the Wufeng–Longmaxi Formations as the primary study objects, we revealed the overall pore structure characteristics of the reservoir. The following conclusions were derived:

1. The combination of AFM and gas adsorption experiment can be used to accurately study the pore structure and fractal characteristics of shale.
2. Shale samples have complex structures and significant fractal characteristics. Fractal dimension is positively correlated with specific surface area and TOC of shale samples, weakly positively correlated with micropore volume, and negatively correlated with average pore radius.
3. The fractal dimension of samples from Wufeng, Long 1_1^1 , and Long 1_1^2 was large, and the fractal dimension of samples from Long 1_2 was the smallest. The pores of the shale samples were generally type H2/3, characterized by wedge-, tabular-, and ink-bottle-shaped pores. The three type H3 pore samples corresponded to the three smallest fractal dimension values.
4. The Long 1_1^1 layer and the Wufeng Formation are the most developed reservoirs and have the most developed storage and flow spaces in each sublayer. Combined with geological and engineering knowledge, it is possible to determine whether the Long 1_1^1 layer and Wufeng Formation can be used as the target layers for staged fracturing horizontal well development in this area.

Acknowledgements We thank LetPub (www.letpub.com) for its linguistic assistance during the preparation of this manuscript.

Funding This study was financially supported by the Science and Technology Project of PetroChina Exploration and Production Company (Grant No. 2022kt1001).

Declarations

Conflict interests The author(s) declared no potential conflicts of interest with respect to the research, authorship, and/or publication of this article.

Open Access This article is licensed under a Creative Commons Attribution 4.0 International License, which permits use, sharing, adaptation, distribution and reproduction in any medium or format, as long as you give appropriate credit to the original author(s) and the source, provide a link to the Creative Commons licence, and indicate if changes were made. The images or other third party material in this article are included in the article's Creative Commons licence, unless indicated otherwise in a credit line to the material. If material is not included in the article's Creative Commons licence and your intended use is not permitted by statutory regulation or exceeds the permitted use, you will

need to obtain permission directly from the copyright holder. To view a copy of this licence, visit <http://creativecommons.org/licenses/by/4.0/>.

References

- Afagwu C, Alafnan S, Mahmoud M, Akkutlu IY (2022) Modeling of natural gas self-diffusion in the micro-pores of organic-rich shales coupling sorption and geomechanical effects. *Natl Gas Sci Eng* 106:104757. <https://doi.org/10.1016/J.JNGSE.2022.104757>
- Afagwu C, Alafnan S, Weijermars R, Mahmoud M (2023) Multiscale and multiphysics production forecasts of shale gas reservoirs: New simulation scheme based on Gaussian pressure transients. *Fuel* 336:127142. <https://doi.org/10.1016/J.FUEL.2022.127142>
- Avnir D, Jaroniec M (1989) An isotherm equation for adsorption on fractal surfaces of heterogeneous porous materials. *Langmuir* 5(6):1431–1433. <https://doi.org/10.1021/la00090a032>
- Blach T, Radlinski AP, Vu P, Ji YP, Campo L, Gilbert EP, Mastalerz M (2021) Deformation of pores in response to uniaxial and hydrostatic stress cycling in Marcellus Shale: implications for gas recovery. *Int J Coal Geol* 248:103867. <https://doi.org/10.1016/J.COAL.2021.103867>
- Cai YD, Li Q, Liu DM, Zhou YF, Lv DW (2018) Insights into matrix compressibility of coals by mercury intrusion porosimetry and N₂ adsorption. *Int J Coal Geol* 200:199–212. <https://doi.org/10.1016/j.coal.2018.11.007>
- Cao TT, Song ZG, Wang SB, Xia J (2016) Characterization of pore structure and fractal dimension of Paleozoic shales from the northeastern Sichuan Basin China. *J Natl Gas Sci Eng* 35:882–895. <https://doi.org/10.1016/j.jngse.2016.09.022>
- Chandra D, Bakshi T, Bahadur J, Hazra B, Vishal V, Kumar S, Singh TN (2023) Pore morphology in thermally-treated shales and its implication on CO₂ storage applications: A gas sorption, SEM, and small-angle scattering study. *Fuel* (P2) 331:125877. <https://doi.org/10.1016/J.FUEL.2022.125877>
- Chandra D, Vishal V, Bahadur J, Agrawal AK, Das A, Hazra B, Sen D (2022) Nano-scale physicochemical attributes and their impact on pore heterogeneity in shale. *Fuel* 314:123070. <https://doi.org/10.1016/J.FUEL.2021.123070>
- Chao Y, Jin CZ, S BH, Zhen GW, (2016) Compositional controls on pore-size distribution by nitrogen adsorption technique in the Lower Permian Shanxi Shales, Ordos Basin. *J Natl Gas Sci Eng* 34:1369–1381. <https://doi.org/10.1016/j.jngse.2016.08.026>
- Chao Y, Jinchuan Z, Shuang BH, Zhen GW (2016) Compositional controls on pore-size distribution by nitrogen adsorption technique in the Lower Permian Shanxi Shales, Ordos Basin. *Natl Gas Sci Eng* 34:1369–1381. <https://doi.org/10.1016/j.jngse.2016.08.026>
- Chen K, Zhang TS, Chen XH, Liang X (2018) Model construction of micro-pores in shale: a case study of Silurian Longmaxi Formation shale in Dianqianbei area, SW China. *Pet Explorat Dev* 45(3):396–405. [https://doi.org/10.1016/S1876-3804\(18\)30046-6](https://doi.org/10.1016/S1876-3804(18)30046-6)
- Chen SB, Gong Z, Li XY, Wang HJ, Wang Y, Zhang YK (2021) Pore structure and heterogeneity of shale gas reservoirs and its effect on gas storage capacity in the Qiongzhusi Formation. *Geosci Front* 12(6):101244. <https://doi.org/10.1016/J.GSF.2021.101244>
- Debanjan C, Vikram V, Jitendra B, Debasis S (2020) A novel approach to identify accessible and inaccessible pores in gas shales using combined low-pressure sorption and SAXS/SANS analysis. *Coal Geol* 228:103556. <https://doi.org/10.1016/j.coal.2020.103556>
- Fatah A, Ben MH, Bennour Z, Gholami R, Hossain M (2022) The impact of supercritical CO₂ on the pore structure and storage capacity of shales. *Natl Gas Sci Eng* 98:104394. <https://doi.org/10.1016/J.JNGSE.2021.104394>
- Fan YC, Liu KY, Pu XG, Zhao JH (2022) Morphological classification and three-dimensional pore structure reconstruction of shale oil reservoirs: a case from the second member of Paleogene Kongdian Formation in the Cangdong Sag, Bohai Bay Basin East China. *Pet Explorat Dev*. [https://doi.org/10.1016/S1876-3804\(22\)60334-3](https://doi.org/10.1016/S1876-3804(22)60334-3)
- Feng Y, Zheng FN, Qing W, Bernhard MK (2016) Pore structure characteristics of lower Silurian shales in the southern Sichuan Basin, China: Insights to pore development and gas storage mechanism. *Coal Geol* 156:12–24. <https://doi.org/10.1016/j.coal.2015.12.015>
- Fu XX, Zhao CP, Lun ZM, Wang HT, Wang M, Zhang DF (2021) Influences of controlled microwave field radiation on pore structure, surface chemistry and adsorption capability of gas-bearing shales. *Marine Pet Geol* 130:105134. <https://doi.org/10.1016/J.MARPETGEO.2021.105134>
- Han H, Cao Y, Chen SJ, Lu JG, Huang CX, Zhu HH, Zhan P, Gao Y (2016) Influence of particle size on gas-adsorption experiments of shales: An example from a Longmaxi Shale sample from the Sichuan Basin, China. *Fuel* 186:750–757. <https://doi.org/10.1016/j.fuel.2016.09.018>
- Hu J, Tang S, Zhang S (2016) Investigation of pore structure and fractal characteristics of the Lower Silurian Longmaxi shales in western Hunan and Hubei Provinces in China. *J Natl Gas Sci Eng* 28:522–535. <https://doi.org/10.1016/j.jngse.2015.12.024>
- Hui H, Chen G, Ning-ning Z, Yuan G (2020) A study on fractal characteristics of lacustrine shales of Qingshankou Formation in the Songliao Basin, northeast China using nitrogen adsorption and mercury injection methods. *Pet Sci Eng* 193:107378. <https://doi.org/10.1016/j.petrol.2020.107378>
- Hui H, Yan C, Shi JC, Yuan G (2016) Influence of particle size on gas-adsorption experiments of shales: an example from a Longmaxi Shale sample from the Sichuan Basin China. *Fuel* 186:750–757. <https://doi.org/10.1016/j.fuel.2016.09.018>
- Iqbal O, Padmanabhan ES, Mandal A, Dvorkin J (2021) Characterization of geochemical properties and factors controlling the pore structure development of shale gas reservoirs. *Pet Sci Eng* 206:109001. <https://doi.org/10.1016/J.PETROL.2021.109001>
- Jing AH, Shu HT, Song HZ (2016) Investigation of pore structure and fractal characteristics of the Lower Silurian Longmaxi shales in western Hunan and Hubei Provinces in China. *Natl Gas Sci Eng* 28:522–535. <https://doi.org/10.1016/j.jngse>
- Kouqi L, Mehdi O, Liangwei S, Reza R (2019) A comprehensive pore structure study of the Bakken Shale with SANS, N₂ adsorption and mercury intrusion. *Fuel* 245:274–285. <https://doi.org/10.1016/j.fuel.2019.01.174>
- Li ZQ, Shen X, Qi ZY, Hu RL (2018) Study on the pore structure and fractal characteristics of marine and continental shale based on mercury porosimetry, N₂ adsorption and NMR methods. *J Natl Gas Sci Eng* 53:12–21. <https://doi.org/10.1016/j.jngse.2018.02.027>
- Li ZQ, Shen X, Qi ZY, Hu RL (2018) Study on the pore structure and fractal characteristics of marine and continental shale based on mercury porosimetry, N₂ adsorption and NMR methods. *Natl Gas Sci Eng* 53:12–21. <https://doi.org/10.1016/j.jngse.2018.02.027>
- Liu K, Ostadhassan M (2017) Multi-scale fractal analysis of pores in shale rocks. *J Appl Geophys* 140:1–10. <https://doi.org/10.1016/j.jappgeo.2017.02.028>
- Liu T, Xiong S, Yu J, He Y, Song P, Chu S, Lin W, Hou H (2021) Study on the microscopic pore structures of the four different kinds of lithological reservoirs in the basin of Western China. *J Pet Explor Prod Technol* 11:1139–1153. <https://doi.org/10.1007/s13202-021-01125-1>
- Medek J, Weishauptova Z (2000) The microporous phase of carbonaceous substances and its fractal dimension. *Fuel* 79(13):1621–1626. [https://doi.org/10.1016/S0016-2361\(00\)00014-4](https://doi.org/10.1016/S0016-2361(00)00014-4)
- Medina RBX, Frouté L, Alvarado V, Kovscek AR (2023) Multimodal study of the impact of stimulation pH on shale pore structure,

- with an emphasis on organics behavior in alkaline environments. *Fuel* 331:125649. <https://doi.org/10.1016/J.FUEL.2022.125649>
- Miao Z, Xue HF (2018) Characterization of pore structure and its impact on methane adsorption capacity for semi-anthracite in Shizhuangnan Block, Qinshui Basin. *Natl Gas Sci Eng* 60:49–62. <https://doi.org/10.1016/j.jngse.2018.10.001>
- Mudoi MP, Sharma P, Khichi AS (2022) A review of gas adsorption on shale and the influencing factors of CH₄ and CO₂ adsorption. *Pet Sci Eng*. <https://doi.org/10.1016/J.PETROL.2022.110897>
- Pang P, Han H, Hu L, Guo C, Gao Y, Xie Y (2021) The calculations of pore structure parameters from gas adsorption experiments of shales: which models are better? *Natl Gas Sci Eng* 94:104060. <https://doi.org/10.1016/J.JNGSE.2021.104060>
- Penghui S, Zhaohui X, Ping W, Liangchao Q, Xiangwen K, Wenguang Z (2019) Investigation of pore structure and fractal characteristics in an organic-rich shale gas-condensate reservoir from the duvernay formation. In: SPE 195527, the SPE Europec featured at 81st EAGE conference and exhibition held in London, England, UK, 3–6 June
- Pfeifer P, Wu YJ, Cole MW (1989) Multilayer adsorption on a fractally rough surface. *Phys Rev Lett* 62(17):1997–2000
- Pitcher EG, Large DJ, Fletcher RS, Rigby SP (2021) Multi-scale pore structural change across a paleodepositional transition in Utica shale probed by gas sorption overcondensation and scanning. *Marine Pet Geol* 34:105348. <https://doi.org/10.1016/J.MARPE.TGEO.2021.105348>
- Qiu HY, Jiang ZX, Liu ZH, Chang JiQ SuZF, Yang ZW, Zhou W (2021) Difference in pore structure characteristics between condensate and dry shale gas reservoirs: insights from the pore contribution of different matrix components. *Natl Gas Sci Eng* 96:104283. <https://doi.org/10.1016/J.JNGSE.2021.104283>
- Saeed SA, Taura U, Al-Wahaibi Y, Al-Muntaser AA, Yuan C, Varfolomeev M, Busaidi RS (2022) Hydrothermal conversion of oil shale: synthetic oil generation and micro-scale pore structure change. *Fuel* 312:122786. <https://doi.org/10.1016/J.FUEL.2021.122786>
- Sakhaee-Pour A, Li WF (2016) Fractal dimensions of shale. *J Natl Gas Sci Eng*. 30:578–582. <https://doi.org/10.1016/j.jngse.2016.02.044>
- Seely R, Liddy TJ, Rochelle CA, Fletcher RS, Rigby SP (2022) Evolution of the mineralogy, pore structure and transport properties of Nordland Shale following exposure to supercritical carbon dioxide. *Pet Sci Eng*. 8(6):562–575. <https://doi.org/10.1016/J.PETROL.2022.110466>
- Shen R, Xiong W, Lang XM, Wang L, Guo HK, Zhou HT, Yang H (2021) Quantitative analysis of nano-scale pore structures of broad sense shale oil reservoirs using atomic force microscopy. *Energy Explor Exploit* 39(6):1839–1856. <https://doi.org/10.1177/01445987211022522>
- Shen R, Zhang XY, Ke YB, Xiong W, Guo HK, Liu GH, Yang H (2021) An integrated pore size distribution measurement method of small angle neutron scattering and mercury intrusion capillary pressure. *Sci Rep* 11:17458. <https://doi.org/10.1038/S41598-021-97027-7>
- Sing KSW (2013) Reporting physisorption data for gas/solid systems with special reference to the determination of surface area and porosity (Recommendations 1984). *Pure Appl Chem*. 57(4):603–619. <https://doi.org/10.1351/pac198557040603>
- Wang J, Liu L, Cui Z, Wang H, Li T, Duan L, Cheng Y, Su P, Li M, Wei X (2021) Multi-fractal characteristics of pore structure for coal during the refined upgrading degassing temperatures. *J Pet Explor Prod Technol* 11:2931–2942. <https://doi.org/10.1007/s13202-021-01226-x>
- Xian FL, Da ZS, Xue QH, Kai D (2019) Nanopore structure of deep-burial coals explored by AFM. *Fuel*. 246:9–17. <https://doi.org/10.1016/j.fuel.2019.02.090>
- Xu H, Zhou W, Zhang R, Qiu MZ (2019) Characterizations of pore, mineral and petrographic properties of marine shale using multiple techniques and their implications on gas storage capability for Sichuan Longmaxi gas shale field in China. *Fuel*. 241:360–371. <https://doi.org/10.1016/j.fuel.2018.12.035>
- Xiong J, Li Y, Zhou S, Liu X, Han H, Liang L, Zhao J (2022) Insights into the pore structure characteristics of the Lower Silurian Longmaxi formation shale in the Jiaoshiba area, Southern Sichuan Basin China. *J Pet Explor Prod Technol* 12:2857–2868. <https://doi.org/10.1007/s13202-022-01486-1>
- Yang F, Wang F, Du J, Yang S, Wen R (2023) Fractal characteristics of artificially matured lacustrine shales from Ordos Basin, West China. *J Pet Explor Prod Technol* 13:1703–1713. <https://doi.org/10.1007/s13202-023-01637-y>
- Zapata YL, Sakhaee-Pour A (2016) Modeling adsorption–desorption hysteresis in shales: acyclic pore model. *Fuel*. 81:557–565. <https://doi.org/10.1016/j.fuel.2016.05.002>
- Zhang J, Tang Y, He D, Zou XY (2020) Full-scale nanopore system and fractal characteristics of clay-rich lacustrine shale combining FE-SEM, nano-CT, gas adsorption and mercury intrusion porosimetry. *Appl Clay Sci* 196:105758. <https://doi.org/10.1016/j.clay.2020.105758>
- Zhu WB, Zhang XH, Zhou DR, Fang CQ, Li JQ, Huang ZQ (2021) New cognition on pore structure characteristics of Permian marine shale in the Lower Yangtze region and its implications for shale gas exploration. *Natl Gas Industry B* 49(5):1085–1097. <https://doi.org/10.1016/J.NGIB.2021.11.004>

Publisher's Note Springer Nature remains neutral with regard to jurisdictional claims in published maps and institutional affiliations.